

Thermalization via Heat Radiation of an Individual Object Thinner than the Thermal Wavelength

C. Wuttke and A. Rauschenbeutel*

Vienna Center for Quantum Science and Technology, TU Wien-Atominstitut, Stadionallee 2, 1020 Wien, Austria

(Received 28 January 2013; published 9 July 2013)

Modeling and investigating the thermalization of microscopic objects with arbitrary shape from first principles is of fundamental interest and may lead to technical applications. Here, we study, over a large temperature range, the thermalization dynamics due to far-field heat radiation of an individual, deterministically produced silica fiber with a predetermined shape and a diameter smaller than the thermal wavelength. The temperature change of the subwavelength-diameter fiber is determined through a measurement of its optical path length in conjunction with an *ab initio* thermodynamic model of the fiber structure. Our results show excellent agreement with a theoretical model that considers heat radiation as a volumetric effect and takes the emitter shape and size relative to the emission wavelength into account.

DOI: 10.1103/PhysRevLett.111.024301

PACS numbers: 44.40.+a, 65.80.-g, 78.67.Uh

Thermalization via heat radiation is an omnipresent process which, e.g., determines the temperature of stars and planets or the functioning of incandescent lamps. For a perfectly black body, the spectral emissive power of far-field thermal radiation was first explained by Planck [1] who used quantized energies for the radiation field, thereby breaking the grounds for quantum theory. The thermal radiation of a real object can then be related to that of a perfectly black body by introducing a correction factor, the so-called spectral emissivity which is treated as a surface property that depends on the specific material and the surface roughness [2]. However, as Planck already stated himself, his theory is designed to describe the far-field heat radiation of macroscopic bodies. Strictly speaking, it cannot therefore be applied to objects that have a size or separation comparable to the thermal wavelength. In particular, as soon as the absorption length for the thermal spectrum gets comparable or larger than the size of the radiating body, thermal radiation becomes a volumetric effect and the spectral emissivity has to take the photonic properties of the object into account. These effects call for a more comprehensive theoretical description. Two established theoretical frameworks in this context are Mie scattering in combination with Kirchhoff's law and fluctuational electrodynamics (FED) [3–6]. Both approaches give accurate predictions for the far-field thermal radiation [6] which, in the case of the infinite cylinder, have formally been shown to be identical [7]. In addition, the FED framework has proven to be a versatile tool which also allows one to compute Casimir forces and the radiative heat transfer of arbitrarily shaped bodies in the far- and near-field [8].

The radiative heat exchange of particles smaller than the thermal wavelength has been extensively studied in the past with ensembles of, e.g., soot particles or interstellar dust in the context of climate physics and astrophysics, respectively [4,9]. In general, these ensembles are not

monodisperse, meaning that only statistical information on their size, shape, and material properties is available. More recently, the progress in nanofabrication led to a new approach using deterministically produced samples of well-defined shape and material. This way, the effect of size and geometrical structure of an object on the spectrum, coherence, and angular distribution of its far-field thermal radiation has been investigated [10–14]. Moreover, it has been shown that the radiative heat transfer rate can be strongly enhanced by near-field effects [15].

Here, we measure the thermalization dynamics of an individual object of predetermined size and shape which is thinner than the thermal wavelength and all absorption lengths of the relevant part of the thermal radiation spectrum. For this purpose, we employ a silica nanofiber with a diameter of 500 nm and monitor its temperature-dependent optical path length interferometrically during heating and cooling. The fiber resides in an ultrahigh vacuum chamber and heat transport is dominated by far-field heat radiation. Our data show that the total far-field radiated power of this subwavelength structure agrees quantitatively with *ab initio* predictions given by FED [7] for temperatures ranging from room temperature up to and beyond the glass transition temperature of fused silica.

The silica nanofibers used for our experiment are realized as the waist of a tapered optical fiber (TOF) which is produced from a standard optical fiber in a heat-and-pull process [16,17]. A temperature change of the nanofiber waist induces a change of its optical path length which is primarily due to the thermo-optic effect of silica. In order to measure this optical path length change, the TOF is enclosed in a fiber-based Fabry-Pérot-type optical resonator which uses two fiber Bragg gratings (FBGs) as cavity mirrors [18]; see inset of Fig. 1.

In this configuration, the optical path length change is translated into a frequency shift of the Fabry-Pérot

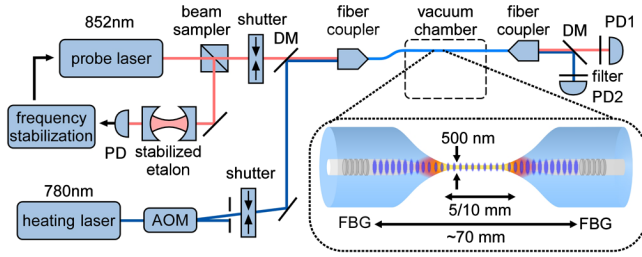


FIG. 1 (color online). Schematics of the experimental setup for measuring the thermally induced optical path length change of the optical nanofiber. The inset shows the TOF resonator with the nanofiber waist.

resonances which we read out via the transmission of a probe laser field; see Fig. 1. The nanofiber waist is heated by sending a second laser field through the TOF. Its wavelength lies in the transmission band of the FBGs and its power is adjustable by means of an acousto-optic modulator (AOM). A small fraction of this optical power is absorbed along the nanofiber, thereby heating the latter. After exiting the TOF, the transmitted probe and heating laser fields are separated by a dichroic mirror (DM) and spectral filters such that their respective powers can be measured independently using photodiodes (PD1 and PD2). By abruptly switching the heating laser beam with a mechanical shutter, the heat source can be turned on and off, allowing us to measure the heating and cooling dynamics of the nanofiber.

For this purpose, we record a time trace of the probe transmission which consists of a sequence of Fabry-Pérot transmission peaks. From one peak to the next, the

single-pass intracavity optical path length has changed by half the vacuum wavelength of the probe laser, $\Delta L_{\text{opt}} = \lambda_0/2 = 426$ nm. A typical time trace of ΔL_{opt} is shown in Fig. 2(a) for a TOF resonator with a waist diameter of (500 ± 50) nm, a nominal homogeneous waist length of $L_{\text{waist}} = 10$ mm, and a finesse of 85 ± 1 [TOF resonator no. 1; see Supplemental Material for a detailed radius profile [19]]. For this measurement, the heating laser is switched on between $t = 0, \dots, 1$ s, the transmitted power is $P_{\text{heat}} = 32.7(1)$ mW, and the background gas pressure is $p = 10^{-6}$ mbar. For both the heating and cooling process, ΔL_{opt} varies rapidly during the first 500 ms. Following this initial fast dynamics, the variation of ΔL_{opt} takes place on a much longer time scale on the order of several seconds. Because of the discrete nature of the measurement method which relies on counting transmission peaks, one additional data point was added at the end of the heating (cooling) period. Its value is chosen $\lambda_0/4$ higher (lower) than the last measured data point and its error bar is given by $\pm \lambda_0/4$, thereby accounting for the fact that ΔL_{opt} changed by less than $\lambda_0/2$.

In order to gain quantitative understanding of the observed dynamics of ΔL_{opt} , we develop an *ab initio* thermodynamical model of the TOF including heat transport via thermal radiation and heat conduction along the TOF. We experimentally checked that heat diffusion through the surrounding background gas is negligible for pressures below 10^{-4} mbar (see below). Moreover, we assume that the fiber is thermalized across its cross section. The system can then be described by the following differential equation in units of power [20]:

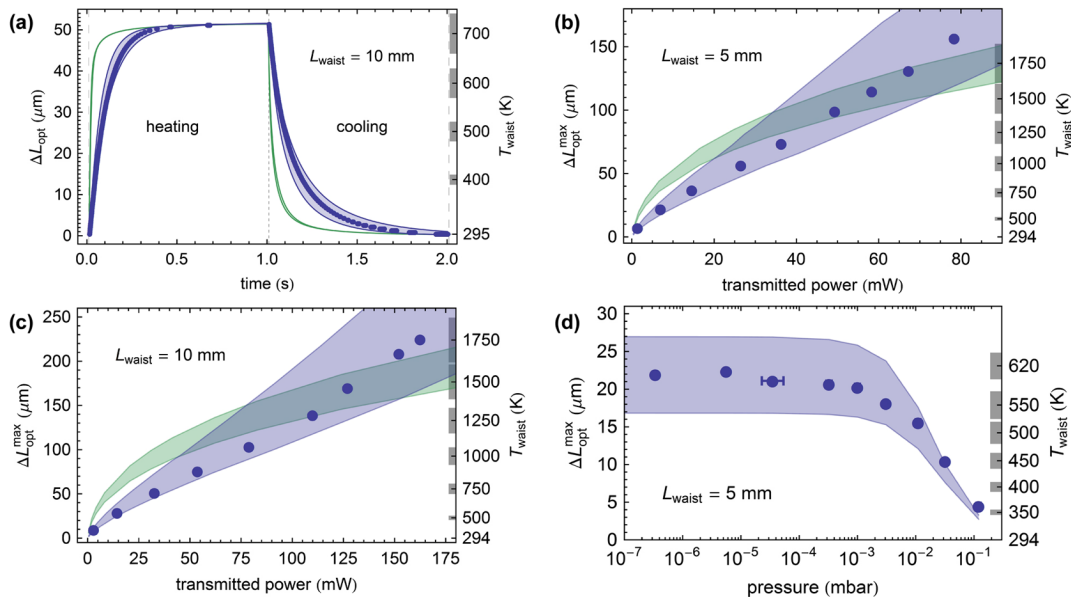


FIG. 2 (color online). Thermally induced optical path length change of the silica nanofiber. Circles, experimental data; blue bands, FED predictions; green bands, predictions using Planck's law. (a) Example of thermalization dynamics. (b)–(d) Maximum optical path length change as a function of the heating laser power transmitted through the TOF and background gas pressure, respectively.

$$c_p \rho \partial_t T dV = -dH_{\text{rad}}(T) + dH_{\text{rad}}(T_0) + \nabla(\lambda \nabla T) dV + dP_{\text{heating}}, \quad (1)$$

where $c_p = (700\text{--}1500)$ J/(kg K) and $\rho = 2200$ kg/m³ are the specific heat and density of silica [21,22], dP_{heating} is a heat source, $\lambda = (1.3\text{--}2.1)$ W/(K m) is the heat conductivity of silica [22], and $T_0 = (294 \pm 0.5)$ K is the room temperature. The dependencies on space and time are omitted for clarity. For comparison, the radiated heat dH_{rad} is calculated using both a naive approach given by Planck's law in combination with the spectral emissivity of a silica-vacuum interface (see Supplemental Material [19]) and the predictions from FED calculations as computed in [7] (details in the Supplemental Material [19]).

It has been shown that the transmission loss of silica nanofibers is primarily governed by surface pollution [23]. In our model, we therefore assume that the heating of the TOF is caused by surface absorption. We note, however, that our analysis only weakly depends on this assumption and that the other extreme case of heating by pure volume absorption yields practically the same results. Despite the fact that the absorption of the heating laser is dominated by pollutants, the overall emittance of the fiber is well described by assuming a pure silica fiber (see Supplemental Material [19]): In essence, the absorption of the pollutant in the near-infrared [$\sim (0.7\text{--}2)$ μm] spectral range only dominates because of the extreme transparency of the silica. However, it is still extremely small and, in particular, negligible compared to that of silica in the wavelength range where the latter is opaque. As a result, the emittance of the total structure (silica nanofiber including the pollutants) is dominated by the properties of silica in the relevant spectral regions, i.e., where the vast majority of the heat radiation is emitted.

The largest uncertainties that enter into the model are the radius profile, which is known with a relative error of $\pm 10\%$ [24,25], and the wavelength-dependent complex refractive index of fused silica \hat{n} . The latter is the sole material property that is used in the FED calculation of the radiated power as well as in the calculation of the spectral emissivity. It was extracted from various literature sources for wavelengths ranging from ≈ 30 nm to ≈ 2 mm (see Supplemental Material [19]).

We numerically solve the two resulting differential equations (Planck and FED) for the same heating and cooling cycle as in the experiment and determine the time-dependent temperature profile along the TOF as a function of the total absorbed optical power P_{abs} . Four different parameter sets are used for these calculations, combining the minimum and maximum TOF radius profile with the values of \hat{n} that yield the minimum or maximum radiated power per unit length, respectively. From these temperature profiles, we then compute ΔL_{opt} via the temperature-dependent effective refractive index which is integrated along the TOF resonator (see Supplemental

Material [19]). The theory bands in Fig. 2(a) are delimited by the two extremal time traces of ΔL_{opt} that reproduce the maximum observed optical path length change $\Delta L_{\text{opt}}^{\text{max}}$ (solid lines). We find excellent agreement between the time dependence of ΔL_{opt} predicted by FED and the experimental data, while the prediction for Planck's law predicts a considerably faster thermalization.

Figures 2(b) and 2(c) show $\Delta L_{\text{opt}}^{\text{max}}$ as a function of the heating laser power transmitted through the TOF, P_{heat} , for TOF resonators 1 and 2. The latter corresponds to a TOF with a waist diameter of (500 ± 50) nm, $L_{\text{waist}} = 5$ mm, and a finesse of 18 ± 1 . In both cases, $\Delta L_{\text{opt}}^{\text{max}}$ increases roughly linearly with P_{heat} within the observed power range. In order to analyze the measured data, the ratio η between P_{heat} and P_{abs} has to be determined. This is done by inserting $P_{\text{abs}} = \eta P_{\text{heat}}$ into both theories and fitting their predictions independently to the data using the four parameter sets concerning the radius and the complex refractive index. We compute the mean of the minimum and maximum resulting η value, $\bar{\eta} = (\eta_{\text{max}} + \eta_{\text{min}})/2 \approx 0.2\%$ for FED and $\bar{\eta} \approx 3\%$ for Planck's law and plot the extremal theory prediction (solid lines bounding the colored bands) using the corresponding two parameter sets and $P_{\text{abs}} = \bar{\eta} P_{\text{heat}}$. For both resonators, the FED prediction is in excellent agreement with the experimental data while Planck's law predicts a sublinear increase of the equilibrium temperature, and therefore of $\Delta L_{\text{opt}}^{\text{max}}$. This qualitative deviation stems from the different scaling of the radiated power with temperature for the two models: T^4 assuming Stefan-Boltzmann law and $< T^3$ in the case of the FED prediction.

From the temperature profiles along the TOF which lead to the two extremal predictions of $\Delta L_{\text{opt}}^{\text{max}}$, we determine two corresponding extremal predictions for the temperature at the center of the waist, $T_{\text{waist}}^{\text{max}}$ and $T_{\text{waist}}^{\text{min}}$, respectively. The resulting nonlinear temperature scale, $\bar{T}_{\text{waist}} = (T_{\text{waist}}^{\text{max}} + T_{\text{waist}}^{\text{min}})/2$, where $\Delta \bar{T}_{\text{waist}} = (T_{\text{waist}}^{\text{max}} - T_{\text{waist}}^{\text{min}})/2$, is shown on the right-hand axes of all panels of Fig. 2, with the ticks and the gray bars indicating \bar{T}_{waist} and $\Delta \bar{T}_{\text{waist}}$, respectively. It covers a temperature range from room temperature to almost 2000 K. We note that the temperature scale in Fig. 2(a) refers to the cooling process. The corresponding scale for the heating process (not shown for clarity) differs from the latter because two distinct spatial temperature profiles arise during heating and cooling. As a result, the same optical path length change corresponds to two different waist temperatures.

While the upper temperature limit exceeds the glass transition temperature of fused silica of about 1450 K [26], the nanofiber did not fuse. In an additional measurement (see Supplemental Material [19]) the fiber survived temperatures of up to (2515 ± 255) K. A theoretical value for this temperature can be obtained by considering the fiber as a filament with a temperature-dependent viscosity [26,27]. We find the melting dynamics to take place at a

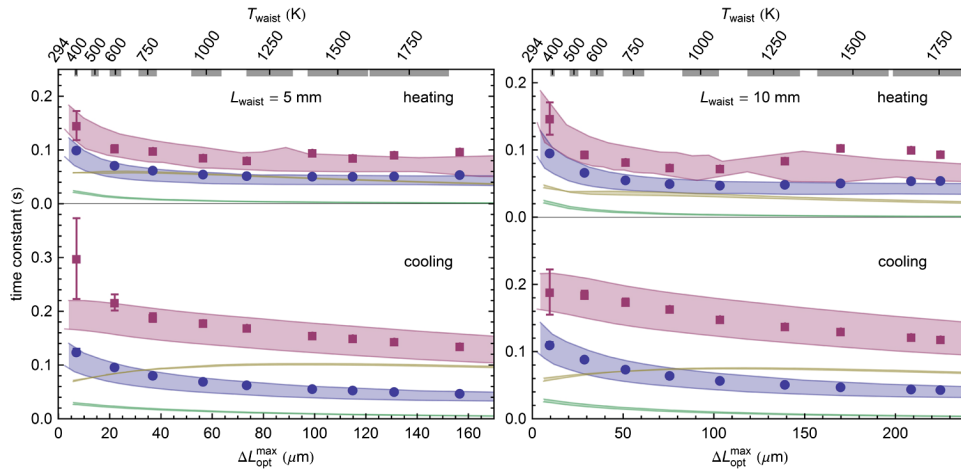


FIG. 3 (color online). Thermalization time constants of the silica nanofiber as a function of the maximum optical path length change for the two TOF resonators. Blue circles, measured initial time constants; red squares, final time constants; blue (red) bands, FED predictions for initial (final) time constants; green (yellow) bands, predictions for initial (final) time constants using Planck's law.

comparable time scale as the experiment, meaning that the fiber would actually break during the experimental cycle, at a temperature of (2710 ± 140) K, which is in good agreement with the experimental result. Based on similar considerations, we also confirmed that the fiber will maintain a minimum stress of ~ 100 kPa during the experiments if the maximum temperature is ~ 1800 K (see Supplemental Material [19]).

Figure 2(d) shows $\Delta L_{\text{opt}}^{\text{max}}$ measured as a function of the background gas pressure for TOF resonator no. 2 and $P_{\text{heat}} = 13.2(4)$ mW. The theory prediction takes heat diffusion through the background gas into account while neglecting temperature gradients. In our experiment, this treatment is valid for pressures smaller than 10^{-3} mbar and overestimates the gas-based heat transport for higher pressures (see Supplemental Material [19]). We find that $\Delta L_{\text{opt}}^{\text{max}}$ is constant for pressures lower than 10^{-4} mbar, confirming that heat diffusion through the background gas is negligible for all other measurements presented here, which were performed at pressures below 10^{-6} mbar.

We now analyze the thermalization dynamics for varying heating powers and thus for varying $\Delta L_{\text{opt}}^{\text{max}}$. For this purpose, we determine the 10%–50% and 75%–90% rise times (heating) and the 90%–50% and 25%–10% fall times (cooling) of the time traces of ΔL_{opt} in order to quantify the initial and the final dynamical behavior. We find time constants on the order of 100 ms which are plotted in Fig. 3 as a function of $\Delta L_{\text{opt}}^{\text{max}}$. The same quantities are derived from the theory predictions for Planck's law and FED, respectively, and plotted as bands in the same graphs. The agreement between the experimental data and the FED predictions is excellent, whereas Planck's law predicts up to 1 order of magnitude shorter time constants and, therefore, highly overestimates the radiated power from the nanofiber. We note that all theory predictions in this figure are *ab initio* results without any adjustable parameters.

Summarizing, using a silica nanofiber of predetermined shape with a diameter smaller than the thermal wavelength, we measured the thermalization dynamics of an individual nanoscopic object over a large temperature range. Our analysis confirms that the total thermally radiated power in the far-field is accurately predicted over a large temperature range using an *ab initio* thermodynamical model based on fluctuational electrodynamics, material properties, and the size and shape of the emitter. Modeling the thermalization of microscopic particles with arbitrary shape from first principles has important applications in the framework of, e.g., heat management in nanodevices, radiative forcing of aerosoles in Earth's atmosphere [28], or cavity optomechanics experiments [29].

We thank M. Rothhardt and co-workers for the FBGs, M. Ponweiser for devising the thermal initialization method, and V. Golyk and M. Krüger for the FED implementation. We acknowledge financial support by the Volkswagen Foundation (Lichtenberg Professorship), the ESF (EURYI Award), NanoSci-E+ (NOIs project), and the Austrian Science Fund (FWF; SFB FoQuS Project No. F 4017).

*Arno.Rauschenbeutel@ati.ac.at.

- [1] M. Planck, *Ann. Phys. (N.Y.)* **309**, 553 (1901).
- [2] R. Siegel and J.R. Howell, *Thermal Radiation Heat Transfer* (McGraw-Hill, New York, 1972).
- [3] S. M. Rytov, Y. A. Kravtsov, and V. I. Tatarskii, *Principles of Statistical Radiophysics* (Springer, Berlin, 1978), Vol. 3.
- [4] C. F. Bohren and D. R. Huffman, *Absorption and Scattering of Light by Small Particles* (Wiley, New York, 1998).
- [5] K. Joulain, J.-P. Mulet, F. Marquier, R. Carminati, and J.-J. Greffet, *Surf. Sci. Rep.* **57**, 59 (2005).

- [6] V. P. Carey, G. Chen, C. Grigoropoulos, M. Kaviany, and A. Majumdar, *Nanoscale Micro. Thermophys. Eng.* **12**, 1 (2008).
- [7] V. A. Golyk, M. Krüger, and M. Kardar, *Phys. Rev. E* **85**, 046603 (2012).
- [8] M. Krüger, T. Emig, and M. Kardar, *Phys. Rev. Lett.* **106**, 210404 (2011).
- [9] T. C. Bond and R. W. Bergstrom, *Aerosol Sci. Technol.* **40**, 27 (2006).
- [10] J.-J. Greffet, R. Carminati, K. Joulain, J.-P. Mulet, S. Mainguy, and Y. Chen, *Nature (London)* **416**, 61 (2002).
- [11] Y. Fan, S. B. Singer, R. Bergstrom, and B. C. Regan, *Phys. Rev. Lett.* **102**, 187402 (2009).
- [12] J. A. Schuller, T. Taubner, and M. L. Brongersma, *Nat. Photonics* **3**, 658 (2009).
- [13] S. Shen, A. Narayanaswamy, and G. Chen, *Nano Lett.* **9**, 2909 (2009).
- [14] X. Liu, T. Tyler, T. Starr, A. F. Starr, N. M. Jokerst, and W. J. Padilla, *Phys. Rev. Lett.* **107**, 045901 (2011).
- [15] E. Rousseau, A. Siria, G. Jourdan, S. Volz, F. Comin, J. Chevrier, and J.-J. Greffet, *Nat. Photonics* **3**, 514 (2009).
- [16] T. A. Birks and Y. W. Li, *J. Lightwave Technol.* **10**, 432 (1992).
- [17] F. Warken, A. Rauschenbeutel, and T. Bartholomäus, *Photonics Spectra* **42**, 73 (2008).
- [18] C. Wuttke, M. Becker, S. Brückner, M. Rothhardt, and A. Rauschenbeutel, *Opt. Lett.* **37**, 1949 (2012).
- [19] See Supplemental Material at <http://link.aps.org/supplemental/10.1103/PhysRevLett.111.024301> for details concerning the thermodynamical model, the modification of the emissivity by pollutants, the material properties of fused silica, and the mechanical stability at high temperatures.
- [20] W. Demtröder, *Experimentalphysik 1* (Springer, Berlin, 2003), 3rd ed., Vol. 1.
- [21] J. Horbach, W. Kob, and K. Binder, *J. Phys. Chem. B* **103**, 4104 (1999).
- [22] J. J. Freeman and A. C. Anderson, *Phys. Rev. B* **34**, 5684 (1986).
- [23] M. Fujiwara, K. Toubaru, and S. Takeuchi, *Opt. Express* **19**, 8596 (2011).
- [24] U. Wiedemann, K. Karapetyan, C. Dan, D. Pritzkau, W. Alt, S. Irsen, and D. Meschede, *Opt. Express* **18**, 7693 (2010).
- [25] A. Stiebeiner, R. Garcia-Fernandez, and A. Rauschenbeutel, *Opt. Express* **18**, 22677 (2010).
- [26] R. H. Doremus, *J. Appl. Phys.* **92**, 7619 (2002).
- [27] J. P. Koulakis, C. D. Mitescu, F. Brochard-Wyart, P.-G. De Gennes, and E. Guyon, *J. Fluid Mech.* **609**, 87 (2008).
- [28] T. C. Bond *et al.*, *J. Geophys. Res. Atmos.* **118**, 1 (2013).
- [29] D. E. Chang, C. A. Regal, S. B. Papp, D. J. Wilson, J. Ye, O. Painter, H. J. Kimble, and P. Zoller, *Proc. Natl. Acad. Sci. U.S.A.* **107**, 1005 (2010).